Heliyon 5 (2019) e02501

Contents lists available at ScienceDirect

Heliyon

journal homepage: www.heliyon.com

Decontamination of ubiquitous harmful microbial lineages in water using an innovative $Zn_2Ti_{0.8}Fe_{0.2}O_4$ nanostructure: dielectric and terahertz properties

Amany Mohamed El Nahrawy [a,*], Ali Belal Abou Hammad [a], Ahmed Mohamed Bakr [b], Bahaa Ahmed Hemdan [c], Ahmed Ramzy Wassel [d]

[a] Solid State Physics Department, Physics Research Division, National Research Centre, 33 El Bohouth St., Dokki, Giza, 12622, Egypt
[b] Spectroscopy Department, Physics Research Division, National Research Centre, 33 El Bohouth St., Dokki, Giza, 12622, Egypt
[c] Water Pollution Research Department, Environmental Research Division, National Research Centre, 33 El-Bohouth St., Dokki, Giza 12622, Egypt
[d] Thin Film and Electron Microscope Department, Physics Research Division, National Research Centre, 33 ElBehouth St., Dokki, Giza, 12622, Egypt

ARTICLE INFO

Keywords:
Condensed matter physics
Materials science
Optics
Condensed matter properties
Materials physics
Environmental pollution
Environmental toxicology
Antimicrobial properties
Dielectric and terahertz spectroscopy
Magnetic nano-perovskite
Disinfectant
Water management

ABSTRACT

Many ubiquitous dangerous microbial lines could originate in different sources of polluted water and be distributed to tap water, which could cause multiple types of illnesses to humans and livestock. Despite enormous attempts to guarantee safety of potable water, these species are still regarded to be threated prevalent health issues and concerns. However, these species need a powerful disinfectant to be removed from contaminated water for receiving clean and healthy water. This study was therefore conducted to produce magnificent magnetic iron titanate zinc nano-particles ($Zn_2Ti_{0.8}Fe_{0.2}O_4$ MNPs) as a sophisticated approach for drinking water (DW) and wastewater purification. The identification of crystalline phase, dielectric and terahertz spectroscopy of iron zinc titanate nanostructure prepared via acidic sol-gel process and calcined at 800 °C. Results show that the formation of cubic structure for Zn_2TiO_4 phase, and the dielectric constant (ε′) decreased with the higher frequency, tan (δ) has higher values at lower frequency and the conductivity increases relatively with frequency that attributes to the high resistive grain boundaries. Absorption coefficient, refractive index and dielectric properties of iron zinc titanate nano-particles was estimated via time domain-terahertz spectrometer and adjusted via the applied electric field. In particular, the Gram-negative bacteria were more prone than other microbes tested to the Magnetic Nano-Particles (MNPs). Results also was ascertained that the minimum inhibitory concentration (MIC) was 25 ppm at 30 min for *E. coli* and *Salmonella enterica*, 45 min for *Listeria monocyteogens, Staphylococcus aureus*, and *Candida albicans* and 60 min for *Aspergillus niger* with a noticeable bactericidal impact. Results exhibit that the MNPs explored are non-toxic and protected for individuals and the environment. MNPs can, therefore, be proposed as an expedient and impressive nano-scale applicant for inactivation during the drinking water and wastewater conservation of the prevailing dangerous microbes.

1. Introduction

Pollution of various water supplies is among the most paramount matters for the supply of water; contaminants can penetrate and transfer to freshwater consumed by mankind [1]. The exclusion of many pollutants, such as organic materials, dangerous microbes and heavy metals, is therefore important for the protection of a secure and clean water system [2]. Drinking water free of maleficent microbes is one of the world's healthiness trouble [3]. The primary source of these undesirable and dangerous contaminants to humans that are released into aquatic settings is raw and insufficiently handled sewage [4]. Many myriad of people were affected by the high concentration of several and various contaminants [5], with many low-income nations opposite a cumbersome challenge in the quality of non-toxic and hygienic water [6].

Wastewater discharge obviously amplified the density of microbial populations in the receiving water streams [7]. Water and wastewater management are a tremendous importance concern of our civilization and other activities [8]. At present, increased requirements of the rank for handled drinking water could also have been achieved through three distinct water treatment methodologies. From these techniques of treatment, chlorine-based disinfection is the greatest crucial practice, and chlorine use is an efficient and economical inhibitor for pathogens.

* Corresponding author.
E-mail address: amany_physics_1980@yahoo.com (A.M. El Nahrawy).

https://doi.org/10.1016/j.heliyon.2019.e02501
Received 6 June 2019; Received in revised form 19 August 2019; Accepted 17 September 2019

Nevertheless, chlorination has some weaknesses which are most important in the occurrence of undesirable decontamination by-products (DBPs) including oncogenic mixtures for instance trihalomethanes (THMs) and haloacetic acids (HAAs), that can be generated, as soon as chlorine interact with natural organic substances (NOMs) [9]. In addition, the existence of some organisms prone to chlorine could increase significantly in water. A sophisticated approach of chlorination which do not form DBPs and is more beneficial toward chlorine-resistant species is therefore strongly recommended for the treatment of water and wastewater [10].

Nanotechnology has been discovered as a hopeful method for drinking water and municipal wastewater decontamination [9] outstanding to the peculiar characteristics of these nano materials. Thus, diverse nanomaterials were synthetized as sanitizer to achieve next-generation requirement of operative, affordable, or sustainable disinfectant in treating water [11]. Among of these nanomaterials, Magnetic Nano-Particles (MNPs) are extensively used for ecological applications, in particular, for decontamination of contaminated water by undesired and harmful microorganisms [12]. Generally, the application of MNPs has established much more considerations because of their distinct properties, for instance tremendously small size, higher surface-area, surface formation, superior magnetic properties and prodigious antimicrobial effects. Moreover, MNPs have been suggseted as disinfectact, nanosorbents and photocatalysts in wastewater management [8]. In addition to MNPs could have eradicating a many types of microbial lineages, including bacteria, parasites, fungi and viruses [13].

Perovskites ($ZnTiO_3$) nano-materials are a group of functional engineering materials and the physico-chemical properties of interest can be rationally tailored to improve electrical and catalytic properties [14]. Perovskites are considered as a hopeful catalysts materials for various industrial processes in purification of non-biodegradable and pre-treated wastewater, micro- and nanoelectronics, ammonia synthesis, dehydrogenization of butylene and decomposition of H_2O_2 and alcohols,.. etc. $ZnTiO_3$ with perovskite structure can be transferred into Zn_2TiO_4 (cubic spinel structure) and TiO_2 by heat treatement or by introducing transition element dopants [14, 15]. Furthermore, preceding studies have demonstrated that such semiconductors (TiO_2, ZnO, $ZnTiO_3$, ...etc) can degrade different kinds of organic pollutants as pesticides, dyes, detergents, and volatile organic composites in dielectric and water and wastewater [16].

Recently, MNPs has been significant interest with various applications of the terahertz frequency regime for characterization and identification of THz radar, biological material, electro-optic coefficients and THz communication with priorities on interaction between the applied electromagnetic radiation and metal oxides and/or biological material [17].

In general, according to the promising using for MNPs in drinking water and domestic wastewater management this study was implemented to study the usage of sol-gel fabricated $Zn_2Ti_{0.8}Fe_{0.2}O_4$, magnetic nanoparticles with cubic spinel structure at lower temperature as a forceful and innovative disinfectant for killing of some ubiquitous harmful microbial lineages during water and wastewater management. Moreover, the studied magnetic nanoparticles $Zn_2Ti_{0.8}Fe_{0.2}O_4$ (MNPs), it can also be used in several applications, such as water decontamination, food packing and biomedical application.

2. Experimental

2.1. Fabrication of magnetic nanoparticles (MNPs)

Iron zinc titanate ($Zn_2Ti_{0.8}Fe_{0.2}O_4$) nanoparticles (magnetic nanoparticles (MNPs) were prepared via sol-gel route. The raw materials used to prepare the nanosized-sample are titanium(IV) isopropoxide Ti $[OCH(CH_3)_2]_4$, zinc acetate $Zn(O_2CCH_3)_2$, and iron(III) nitrate nonahydrate $Fe(NO_3)_3 \cdot 9H_2O$. Certain amounts of iron nitrate and zinc acetate were disbanded in filtered (H_2O) and acetic acid CH_3COOH, while the titanium iso-propoxide was dissolved in acetylacetone ($CH_3COCH_2COCH_3$). After the dissolving process the various solvent mixed together with magnetic stirring. The produced homogeneous solution was dried on hotplate at 200 °C until obtaining a completely xerogel then calcined at 800 °C for 4h. Finally, the obtained nano-powder was grinding into fine nano-powder.

2.2. Characterization

The crystal structure of the $Zn_2Ti_{0.8}Fe_{0.2}O_4$ nanoparticles was characterized via X-ray Bruker- D8 advance diffractometer (XRD- Japan) with monochromatized (CuKα) radiation with λ = 1.54056 Å worked at (40 kV and 40 mA. Surface morphology of the prepared nanopowder was scanned via field emission-scanning electron microscope (FE-SEM), (JEM – 1230; Japan). The dielectric measurements were carried out by using Broad-band Dielectric Spectroscopy (B-BDS, German) type Novocontrol concept 40. The nanopowders were pressed into tablets with thickness 2 mm and 14 mm in diameter in order to carry out the dielectric measurements. The dielectric measurements were carried out by using sample holder with two stainless steel parallel electrodes coated with gold and 10 mm in diameter.

THz Time-Domain Spectroscopy System (TeraView TPS 3000- England), the laser source is a merchant mode-locked Ti:sapphire laser (Spectra Physics Mai Tai) producing 70–120 fs pulses at 780–920 nm with a recurrence level of 80 MHz and a typical power of 600–1200 mW. The fs laser beam was split into two beams, one for stimulating the emitter antenna, and the second one for determining the THz signal at the detector crystal. The THz emitter is a coplanar stripline antenna manufactured on a semi-insulating (SI) GaAs wafer. The gap space of the emitter antenna is 200 μm and is stimulated with a 7-mW of intensive laser beam. The values of the refractive index, n and the absorption coefficient, α of the $Zn_2Ti_{0.8}Fe_{0.2}$ O_4 nano-particles sample are estimated from the evaluated data using the Eqs. (1), (2), (3), (4), (5), and (6). The refractive index, n and the absorption coefficient, α of the $Zn_2Ti_{0.8}Fe_{0.2}$ O_4 nano-particles are evaluated using the recorded data by using Eqs. (2) and (4).

$$T = e^{\frac{(4\pi Kd)}{\lambda}} * \frac{(1-R)^2 + (4R\sin\psi)^2}{\left(\left(1 - Re^{\frac{(4\pi Kd)}{\lambda}}\right)^2 + 4Re^{\frac{(4\pi Kd)}{\lambda}} \sin^2\left(\frac{(2\pi nd)}{\lambda}\right) + \psi\right)} \quad (1)$$

$$R = \frac{K^2 + (n-1)^2}{K^2 + (n+1)^2} \quad (2)$$

$$\alpha(\omega) = \frac{1}{d} \ln \frac{|E_s(\omega)|}{|E_r(\omega)|} \quad (3)$$

$$n = 1 + \frac{[\varnothing_s(\omega) - \varnothing_r(\omega)]c}{d\omega} \quad (4)$$

$$\varepsilon' = \ n^2 - K^2 \quad (5)$$

$$\varepsilon'' = 2nK \quad (6)$$

Where (*T and R*) are the transmission coefficient and the reflection coefficient of the prepared sample, (φ) is the transmitted wave phase shift, (ψ) is the phase shift of the reflected wave, the sample thickness is d, (*n* and *K)* are the refractive index and absorption coefficients, the corresponding amplitude $|E_{sam}(\omega)|$, $|E_{ref}(\omega)|$ and both (ε′ and ε″) are dielectric parameters, respectively.

2.3. Antimicrobial susceptibility test

2.3.1. Zone inhibition test

Three different groups of extremely prevailing harmful pathogenic

microorganisms such as Gram-negative bacteria (*Escherichia coli* ATCC 25922, *Salmonella enterica* serovar typhimurium ATCC 14028), Gram-positive bacteria (*Listeria monocytogenes* ATCC 25152, *Staphylococcus aureus* ATCC) and fungal species (*Candida albicans*, and *Aspergillus niger* local strains) were chosen to evaluate the inhibition efficiency of fabricated MNPs-disinfectant using both disk and well diffusion assays using Mueller Hinton medium (Merck, Germany) [18]. The diameters of inhibition zone (mm) around the disks and wells as inhibitory influences were measured. All experiments in this study were multiplied in three times and were replicated triplicate on different days [18].

2.3.2. Minimal inhibitory concentrations (MIC)

The MIC of MNPs against the mentioned harmful microbial pathogens was estimated by broth dilution methods [19]. The MIC was defined as the minimum concentration of MNPs-disinfectant at which no growth was observed following overnight incubation at 37 °C. Briefly, ten mL sterile distilled water tubes which containing three different concentrations (5, 15 and 25 ppm) of studied MNPs-disinfectant was inoculated by 100 μL of each a 24 hr-microbial culture. Free-disinfectant tubes were done as a control for each mentioned microbial species. All experiments were started under steady conditions in shaking incubator (at 25 °C and 250 rpm of shaking) [20]. For the inactivation effects, one mL of each inoculated tubes was taken at five different contact times (5, 15, 30, 45 and 60 min) for estimation of the viable cell densities using pour plate method according to the literature [21].

The initial counts in all experiments were estimated at zero time. The inactivation efficacy at every exposure time was repeated [22]. The inactivation efficacy was elaborated according to Eq. (7).

$$(I\%) = (C_1\text{-}C_0)/(C_1 x 100). \quad (7)$$

where $I\ \%$ = inactivation efficiency, C_1 = initial counts of microbial strain; C_0 = counts of microbial strain at each sampling time.

2.4. Kinetic modelling for mechanism of action

In order to evaluate the inactivation rate of the tested microbial lineages, the pseudo-first-order equation was expressed for determining the inactivation rate of studied MNPs-disinfectants Eq. (8) [23].

$$\log(q_e - q_t) = \log q_e - \frac{k_1 t}{2.303} \quad (8)$$

where k_1 (1 min^{-1}) is the inactivation rate constant of a pseudo-first-order equation, and q_e ($mg.g^{-1}$) and q_t ($mg.g^{-1}$) define the absorbed amount at equilibrium and at time t (min), respectively. The relation between ln ($q_e - q_t$) and t *represents* a straight line that recommended that this kinetic model is fitting to the gained information.

2.5. Toxicity performance assay

To evaluate the hazardous effects of studied MNPs, the toxicity levels of MNPs-disinfectant were measured via a cytotoxicity methods on the Hep-2 cell line with Microtox Analyzer 500 [24,25].

2.6. Application of MNPs in DW and wastewater management

In disinfection of three distinct kinds of water (Nile water, tap water mixed with target microbes, and raw domestic sewage), the powerful dosage of MNPs was implemented. Some prevalent waterborne pathogens such as *E. coli*, *S. enterica*, *L. monocytogenes*, *S. aureus*, *C. albicans* and *A. niger* were counted before and after adding the dose of disinfectant in the tested water samples. All these pathogens were enumerated using spread plate method by spreading 100 μL of each water sample onto surface of plate containing rapid HiColiform agar, Improved Salmonella agar, Hicrome Aureus agar, Hicrom Listeria selective agar, Hicrome Candida selective agar and Sabouraud Dextrose agar, respectively. All media used were bought from HiMedia Co., India [21].

With the proficient dose of MNPs-disinfectant, three conical bottles every one having 50 mL of Nile water, inoculated tap water and raw wastewater trials were thoroughly cleaned. The flasks were agitated using shaker at 250 rpm and 25 °C. A 100 μL of each flask, which inoculated by tested harmful microbes, was taken within different time intervals as a following; zero, 5, 10, 20, 30, 40, 50 and 60 min, and stretched to the revealed surface of selective agar medium. All injected dishes were subsequently incubated overnight at thermophilic condition (37 °C), and the typical colonies have been calculated [19].

3. Results and discussion

3.1. XRD and FE-SEM studies

XRD Chart of $Zn_2Ti_{0.8}Fe_{0.2}O_4$ shows a well-defined polycrystalline zinc titanate with a cubic spinel structure (A_2BO_4) as present in Fig. 1. The peaks of the obtained cubic structure were indexed according to (JCPDS Card 86-0156) that refers to the cubic spinel Zn_2TiO_4 phase. While the residual peaks refers to the Rutile TiO_2 as indicated in the chart. The XRD chart didn't refer to any other phases containing Fe. This result confirms that the weight amount of Fe is completely replacing the titanium ion inside the structure [26, 27, 28]. The Rutile phase was appeared due to the effect of Fe ion that transferred the perovskite phase

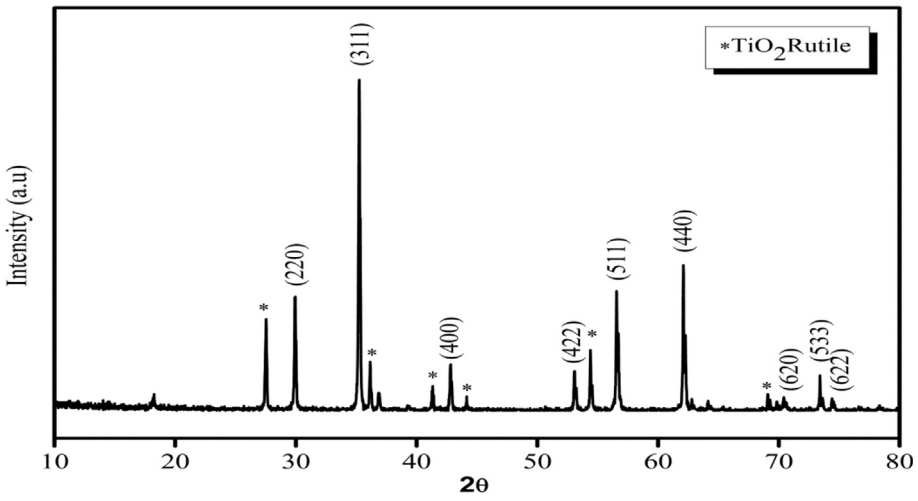

Fig. 1. Shows the indexed XRD of $Zn_2Ti_{0.8}Fe_{0.2}O_4$, calcined at 800 °C.

$ZnTiO_3$ (rhombohedral) to cubic spinel structure Zn_2TiO_4 and Rutile TiO_2.

The average particle size (*D*) was evaluated by Scherrer Eq. (9):

$$D = (k\lambda)/(\beta\cos\theta) \quad (9)$$

Where λ is the X-ray wave length (1.5406 Å), the correction factor k is 0.9 and β is the Full width at half maximum of the selected peak [29]. The average particle size (D) was found to be 53 nm. Eq. (10) was used to evaluate the lattice parameters (a) of the cubic structure of the sample.

$$d_{hkl} = a/(h^2+k^2+l^2)^{0.5} \quad (10)$$

h, k and l are the Millar indices, d is the d-spacing and a is the lattice parameter. The value of lattice parameter a is 8.459 Å, according to Eq. (10). The XRD density (D_x) and is given by

$$D_x = 8M/(N_a{*}a^3) \quad (11)$$

M is the molecular weight of the materials and *N*a is Avogadro's number and

According to the chemical formula of the sample $Zn_2Ti_{0.8}Fe_{0.2}O_4$

$$M = 2\ {*}M_{Zn} + 0.8{*}M_{Ti} + 0.2{*}M_{Fe} + 4{*}M_O = 244.2202\ g/mol$$

M_{Zn}, M_{Ti}, M_{Fe} and M_O are the molecular weight of Zn, Ti, Fe an O. The specific surface area (*SA*) is given by

$$S_A = 6000/(D{*}D_x) \quad (12)$$

The specific surface area was found to be 21.12 m^2/g [30].

The characteristic surface morphology of ZT/20 Fe nano-particles was inspected by the high resolution-scanning electron microscopy (HR-SEM) at two magnifications (20,000x and 80,000x), as seen in Fig. 2. The images reveal that the sample shows a dense arrangement of homogeneous cubic nanoparticles with some spherical shape [14]. The chemical composition for $Zn_2Ti_{0.8}Fe_{0.2}O_4$ sample was confirmed by EDX, as displayed in Fig. (2c).

3.2. Dielectric properties

The dielectric constant of $Zn_2Ti_{0.8}Fe_{0.2}O_4$ decreases with increasing frequency and nearly becomes stable at high frequency, as seen in Fig. 3. The decreasing of the dielectric constant at high frequency is assigned to the disappearance of the effect of some different types of polarizations such as interfacial polarization, orientaional polarization, etc [31, 32]. The behavior of dielectric constant with frequency of $Zn_2Ti_{0.8}Fe_{0.2}O_4$

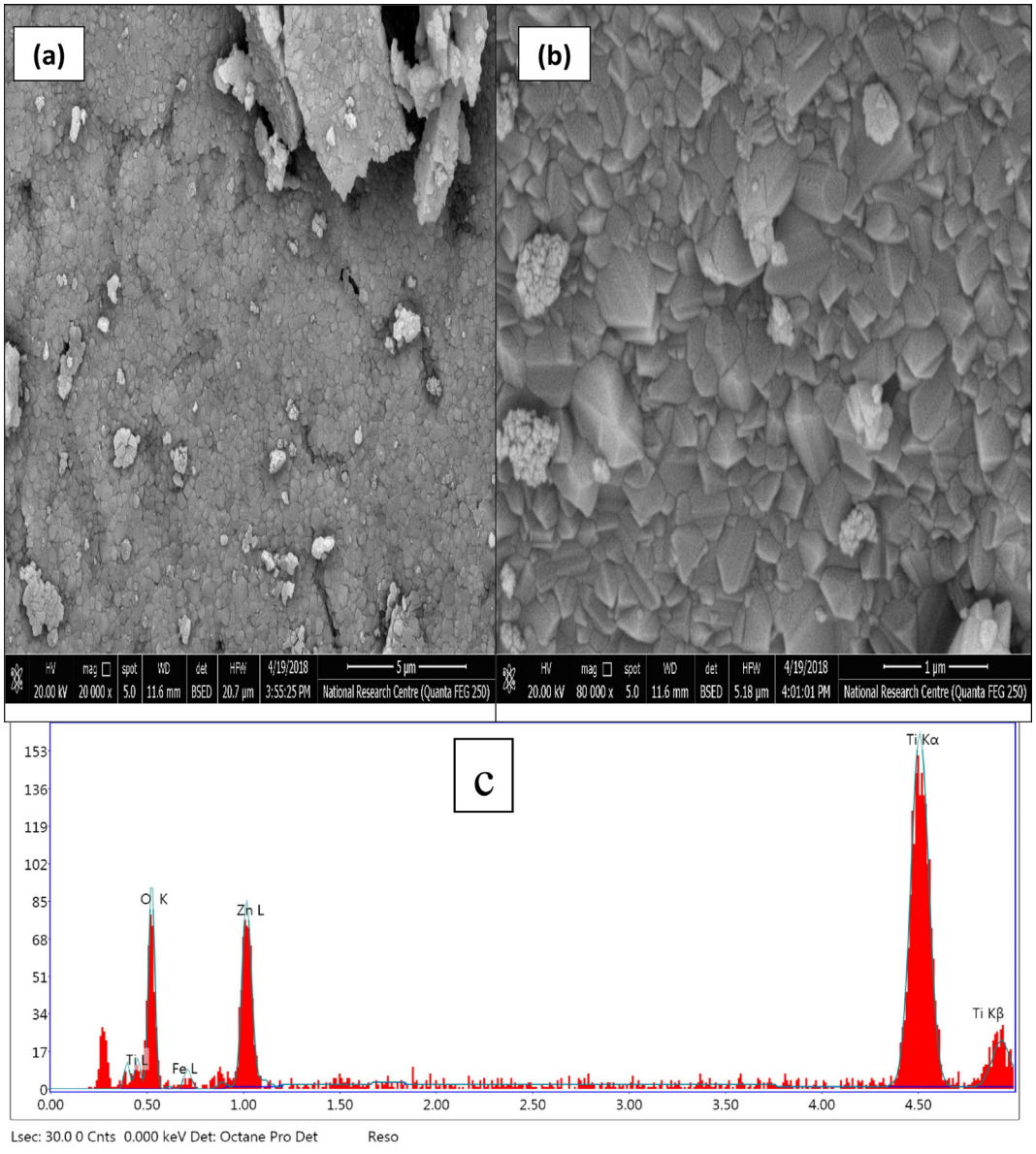

Fig. 2. Shows the FE-SEM of $Zn_2Ti_{0.8}Fe_{0.2}O_4$, calcined at 800 °C at two magnifications (a) 20,000x and (b) 80,000x and (c) EDX.

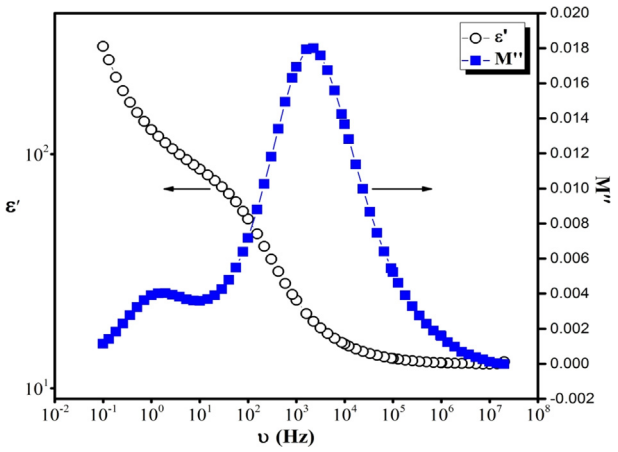

Fig. 3. Shows the frequency dependency of dielectric constant (ε′) versus the imaginary part of dielectric modulus (M″) of $Zn_2Ti_{0.8}Fe_{0.2}$ O_4, calcined at 800 °C.

shows two plateaus in the curve that attributes to the presence of two dielectric relaxation processes in the sample. The first plateau lies in the low frequency up to 100 Hz may be released from the dispersion of interfacial polarization, Maxwell-Wagner model. This model states that polycrystalline ceramics (MNPs) have a varied microstructure in which the insulating grain boundaries surrounding the semiconducting or conducting grains. During the application of an alternating electric field (AC) the charge carriers are going to be collected in the grain boundaries and hence building up the interfacial polarization at low frequency [33]. While, the second plateau may be due to the relaxation of grains itself. The (M″ vs υ) curve shows two peaks distributed over the studied frequency range. The presence of such two peaks confirms the presence of two relaxation processes along the frequency range [34]. The first peak is attributed to the dipolar polarization that results from the interfacial polarization, while, the second peak is attributes to the dipolar polarization results from the grains [35]. The relaxation frequency of the peak at high frequency separates between two mechanisms of conduction. At low frequency zone below the relaxation frequency the conduction is due to hoping over long distance while at high frequency over the relaxation frequency the conduction mechanism is released from short rang hoping [36]. These results are confirmed by the (σ vs υ) curve Fig. 4, where the conductivity curve shows two distinct areas. In the first area the conductivity increases relatively with frequency that attributes to the high resistive grain boundaries. With increasing frequency, the effect of the semiconductive grains becomes dominant and leads to increase conductivity linearly with frequency [37, 38].

Fig. 5 displays the variation of the loss tangent versus frequency. It reveals that loss tangent attains high values at lower frequency and remains nearly constant at high frequency with lower values. In lower frequency range the grain boundaries has the prominent effect in polarization under the direct effect of the external field. So, ceramic sample is highly resistive at low frequency and hence more energy is needed in order to transfer charge carriers. With increasing frequency the loss tangent decreases and then has a peak at 420 Hz. The presence of such peak is owing to the matching between the frequencies of the applied field with the hopping frequency of charge carriers. At high frequency region the effect of grain boundaries decreases and hence small amount of energy is needed for transferring charge carriers. So, loss tangent decrease with frequency [39].

3.3. Terahertz spectroscopy

The values of both refractive index, n and absorption coefficient, α of the highly ordered $Zn_2Ti_{0.8}Fe_{0.2}$ O_4 nano-particles sample are studied from the evaluated data via the Eqs. (1), (2), (3), and (4). The (α) spectrum of the highly ordered $Zn_2Ti_{0.8}Fe_{0.2}O_4$ nano-particles obviously an increasing in the absorption accompanied with shifted towards higher (THz) frequencies (Fig. 6 (a)). The decrease in the absorption losses with the (THz) frequency is due to the creation of relaxation process in the dense structure and higher chain length $Zn_2Ti_{0.8}Fe_{0.2}O_4$ nano-particles sample. The obtained frequency domain data was used to extract the refractive index (n) of the highly ordered $Zn_2Ti_{0.8}Fe_{0.2}O_4$ nano-particles, as shown in Fig. 6 (b). The (n) values at the lower (THz) is higher than at the optically higher frequency, which can predictable that the refractive index values in the terahertz regime to oncoming the optical values at the higher frequencies [40].

The estimated time domain, the Fourier transformed frequency domain and the electric field of terahertz pulses in the highly ordered $Zn_2Ti_{0.8}Fe_{0.2}O_4$ nano-particles sample with their reference (air) are measured in the time domain, and the equivalent frequency spectra are gained from the employ of the numerical Fourier transforms, as presented in Fig. 7 (a,b). Every pulse curve for both the reference and $Zn_2Ti_{0.8}Fe_{0.2}O_4$ nano-particles sample is the average of three subsequently measurements with an approach to increase the ratio of the signal-to-noise. Also, the shift time between the reference (air) and the $Zn_2Ti_{0.8}Fe_{0.2}O_4$ nano-particles was ~0.18 ps. The empirical real (ε′) and imagery (ε″) parameters as a dielectric functions of the prepared sample were calculated using the Eqs. (5) and (6). Form the Fig. 7(c), there is a pronounced relaxation process eventuating in the scale of 0.21–0.53 THz

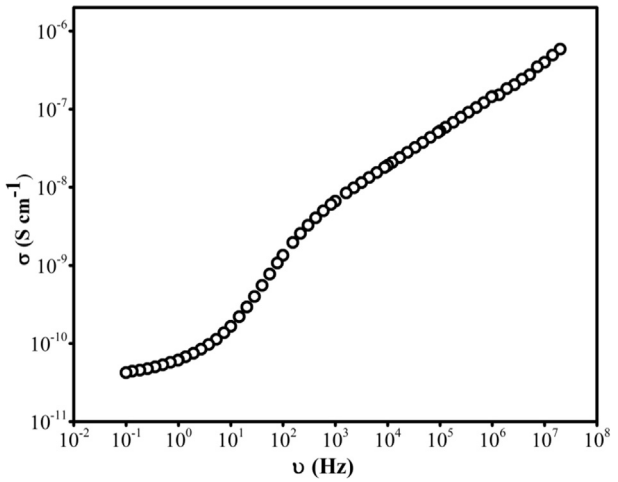

Fig. 4. Shows the frequency dependency of conductivity (σ) of $Zn_2Ti_{0.8}Fe_{0.2}O_4$, calcined at 800 °C.

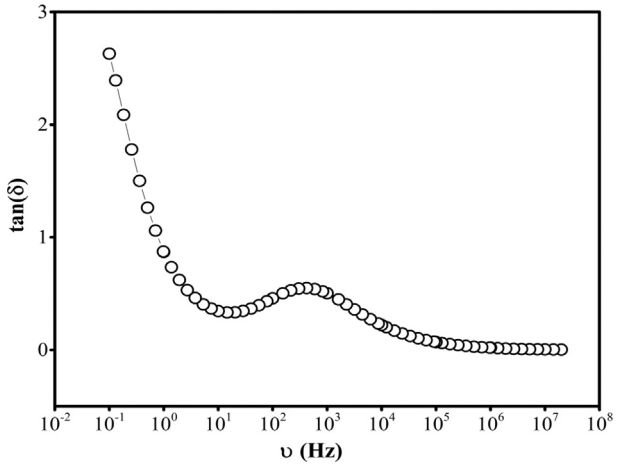

Fig. 5. Shows the loss tangent versus frequency of $Zn_2Ti_{0.8}Fe_{0.2}$ O_4, calcined at 800 °C.

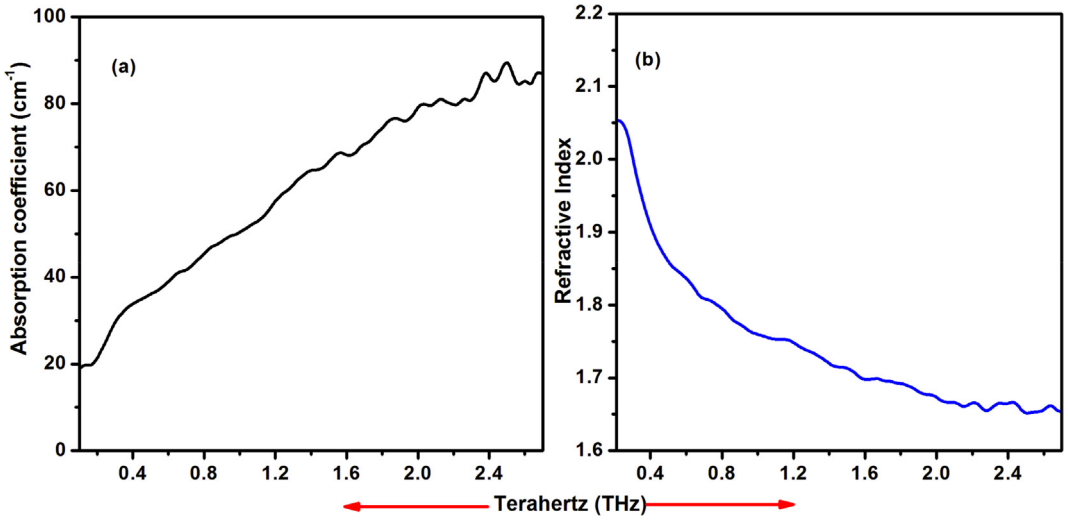

Fig. 6. (a) Absorption coefficient (α) and (b) the refractive index (n) in THz for $Zn_2Ti_{0.8}Fe_{0.2}O_4$ nano-pervoskite.

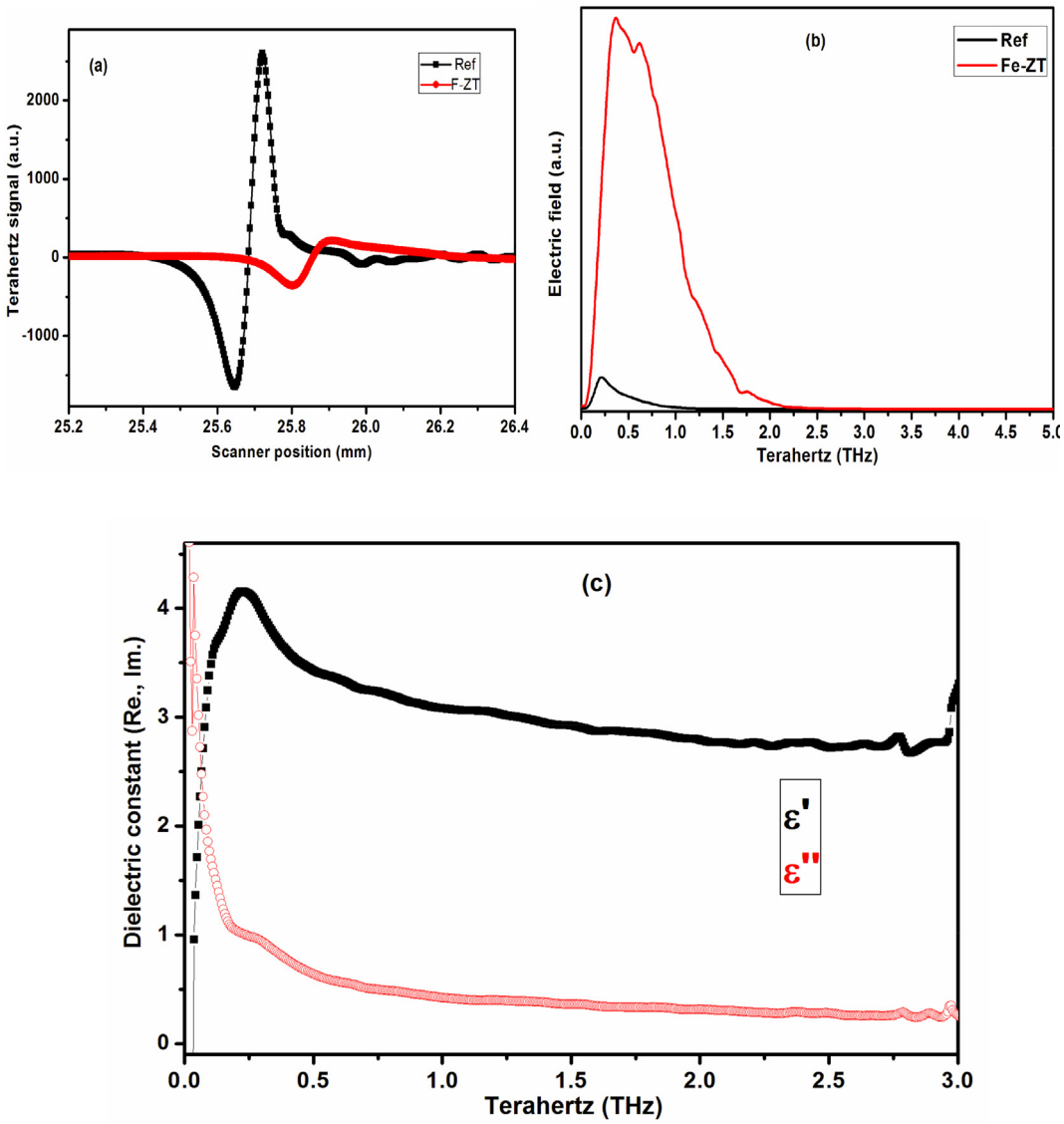

Fig. 7. (a) Time domain THz waveforms, (b) the electric field: Fourier transforms of the corresponding time-domain signals and (c) the real (ε′) and imaginary (ε″) of the dielectric functions for $Zn_2Ti_{0.8}Fe_{0.2}O_4$ nano-pervoskite.

for the $Zn_2Ti_{0.8}Fe_{0.2}O_4$ sample and decreases slightly with the THz frequency. This decrease may be due to the tenuous distortion of $Zn_2Ti_{0.8}Fe_{0.2}O_4$ nano-particles, which indicate the gradually change and the weak infra-red activity in terahertz regime [41].

It's noted that the imaginary dielectric constant (ε″) of the sample decrease slightly and is relatively constant in the higher (THz) frequencies. Which elucidate the high responsive measurements of the infrared active modes enabling from the detection of the weak internal changes in the highly ordered $Zn_2Ti_{0.8}Fe_{0.2}O_4$ nano-particles.

3.4. Antimicrobial susceptibility testing

Iron oxide NP (IONP) is one of the most metallic oxides distributed in nature and simply fabricated. MNPs have a gigantic attention in ecological, biomedical, and water purification applications due to their peculiar properties [42, 43]. In this research, the fabrication of MNPs was based on presence of iron, TiO_2 and Zn. Table 1 shows the effect of fabricated MNPs to some problematic and dangerous microbial lineages using disk and well diffusion methods. Obvious inhibition effects measured by zone diameters were noticed toward all tested microbial lineages. Results unveil that Gram-negative species were more susceptible to MNPs than other tested microbes. The highest inhibition zone diameter reached 14 and 16 mm using disc and well diffusion methods for *S. enterica*, while the lowest diameters reached 10 and 11 mm using disc and well diffusion methods for *A. niger*. Due to the unique structure of studied fabricated MNPs, the highly antimicrobial activity of these nanomaterial caused by the presence of each TiO_2 and Zn was clearly observed against tested harmful microbial lineages. Our results in agree with [44] who stated that TiO_2 able to eradicate both Gram positive and negative bacteria. Moreover, ZnO in nano-scale size displays a forceful antibacterial action on a miscellaneous varieties of bacterial lineages [45, 46]. MNPs are the reliable disinfectant toward *Bacillus subtilis* developing a clear area of 18 mm with regard to the outcomes of the disc diffusion approach. The minimum effect was against *L. monocytogenes* with zone of inhibition (8 mm). The width of given clear zone toward target strains; *S. enterica*, *C. albicans*, *S. aureus*, *E. coli*, *P. aeruginosa*, and *E. faecalis*, respectively were 10, 10, 11, 12, 12, and 12 mm. Furthermore, results in compatible with [19] who revealed that, Clear area widths using well diffusion techniques were larger than that of the disk diffusion technique. In antimicrobial sustainability test, results found that *Staph. aureus* as a Gram-positive bacteria is highly resistant than *E. coli* as a Gram-negative bacteria [46]. In contrast [47], confirmed that *P. aerugenosa* is stronger than *S. aureus* this might to owing to the difference in the dose of MNPs and types of bacterial lineages.

Fig. 8 represents the cell viability and log reduction values of tested microbial lineages exposed to three different doses of MNPs. Different doses of MNPs solution (5, 15, and 25 ppm) significantly decreased the total population densities of the tested microbial lineages. Results display that 25 ppm of MNPs could be fully reduced within 30 min of exposure time for both *E. coli* (from log 6.57 to 0 CFU/ml) and *S. enterica* (from log 6.65 to 0 CFU/ml). While the target Gram-positive species (*S. aureus* and *L. monocytogenes*) and *C. albicans*, the log reduction of microbial densities was wholly removed at 25 ppm of MNPs for 45 min of exposure time. Among of tested microbes, the reduction of *A. niger* form log 6.46 to 0 CFU/ml was relatively the lowest (at 25 ppm for 60 min) when comparing with other tested microbes. It's well-known that TiO_2 is the most frequently nanoparticle used to eliminate dangerous microbes in water sources. The eradication of these microbes depends on numerous issues *e.g.,* dose of TiO_2, type of microbes, strength of light, degree of hydroxylation, pH, temperature, and exposure time [48]. In addition TiO_2 nanopaticle can eliminate harmful miocobial lineages by producing some reactive oxygen species (ROS) [49].

Our results closely similar with [50] revealed that the impact of TiO_2 on five distinct microbial species was researched and the inhibition rate of these bacterial species was as follows; *E. coli* > *P. aeruginosa* > *S. aureus* > *E. faecium* > *C. albicans.* On the other hand, the presence of Zn could be improved the inhibition activities of studied MNPs. Even though ZnO nanoparticles have antimicrobial properties, waterborne pathogenic microbes can be extremely affected. Since ZnO dissolves effortlessly, its applications in water purification will be limited.

Table 1
Inhibition zone testing and clear zone diameters of MNPs against tested harmful microbial lineages.

Tested harmful microbial lineages	Clear zone diameter (mm)	
	Disc diffusion	Well diffusion
E. coli	13 ± 0.23	15 ± 0.21
Salmonella enterica	14 ± 0.18	16 ± 0.24
Staphylococcus aureus	11 ± 0.19	13 ± 0.19
Listeria monocytogenes	12 ± 0.28	14 ± 0.17
Candida albicans	11 ± 0.22	13 ± 0.15
Aspergillus niger	10 ± 0.29	11 ± 0.22

3.5. Application of Pseudo-first-order kinetic model modeling

To better understanding the inactivation rate and the effect of MNPs disinfectant to tested microbial lineages, Pseudo-first-order kinetic model was applied and the k_1 values were calculated from Eq. (8) as shown in Fig. 9 and Table 2. The values of R^2 and k_1 constant pointed out there are a strong correlation with significance between the dose of MNPs (5 and 15 ppm) and the inactivation rate of tested harmful microbial lineages. The order of inactivation rate determined by K_1 constant was in *E. coli* (0.0882)> *S. enterica* (0.0558) > *S. aureus* (0.0379) > *L. monocytogenes* (0.0558) > *C. albicans* (0.0099) ~ *A. niger* (0.0098). Additionally, the rate of inactivation was more rapidly with increasing the dose of MNPs up to 15 ppm. These results in accordance with [22] who used K_1 constant model to express the inactivation rate values of *E. coli* after exposure to photocatalysts.

3.6. Toxicity assays

The experimental results exhibit that MNPs was environmental benign and its EC_{50} was 348 mg/L (>100 mg/L), it means that the tested MNPs could be safe for using in water treatment. These results are compatible with the results of [51]. Besides, the cytotoxicity assay pointed out that MNPs haven't any negative effect toward Hep-2 cell line [52]. Although Cu is regarded as an efficient agent with adequate toxicity to animals [53]. The harmfulness and ecological impact of NPs are ultimate anxieties for choosing of the safeguard disinfectant for safely using in water treatment field. As well, WHO is revealed that Zn concentration lower than 3 mg/l might be applicable to individuals [54]. The toxicity of MNPs is still a fundamental issue of discussion [55].

3.7. Mechanism of action of inactivation

In general, the antimicrobial action of MNPs mainly purposes by three different ways for killing of bacteria: destruction of cell wall; liberating of toxic substances, which causing failure in protein function when react with proteins, and thus eradicating the viable microbial cells; and producing reactive oxygen (ROS), an active reactant that destroy DNA, RNA, and proteins, thus exterminating microbial cells [12]. Gram-positive bacteria have a profound and dense cell wall that contains peptidoglycan and teichoic acids in layers, while gram-negative bacteria have slender and thin peptidoglycan cell walls that comprise by lipopolysaccharides and lipoproteins layers of lipid membranes. MNPs are regarded promising nano-scale materials and revolutionize the ability to manage wastewater [56]. By avoiding their accumulation during implementation, the antimicrobial characteristics of these oxide-based NMs will be improved; consequently, the choice of sufficient scattering agents will still be a complicated mission [9].

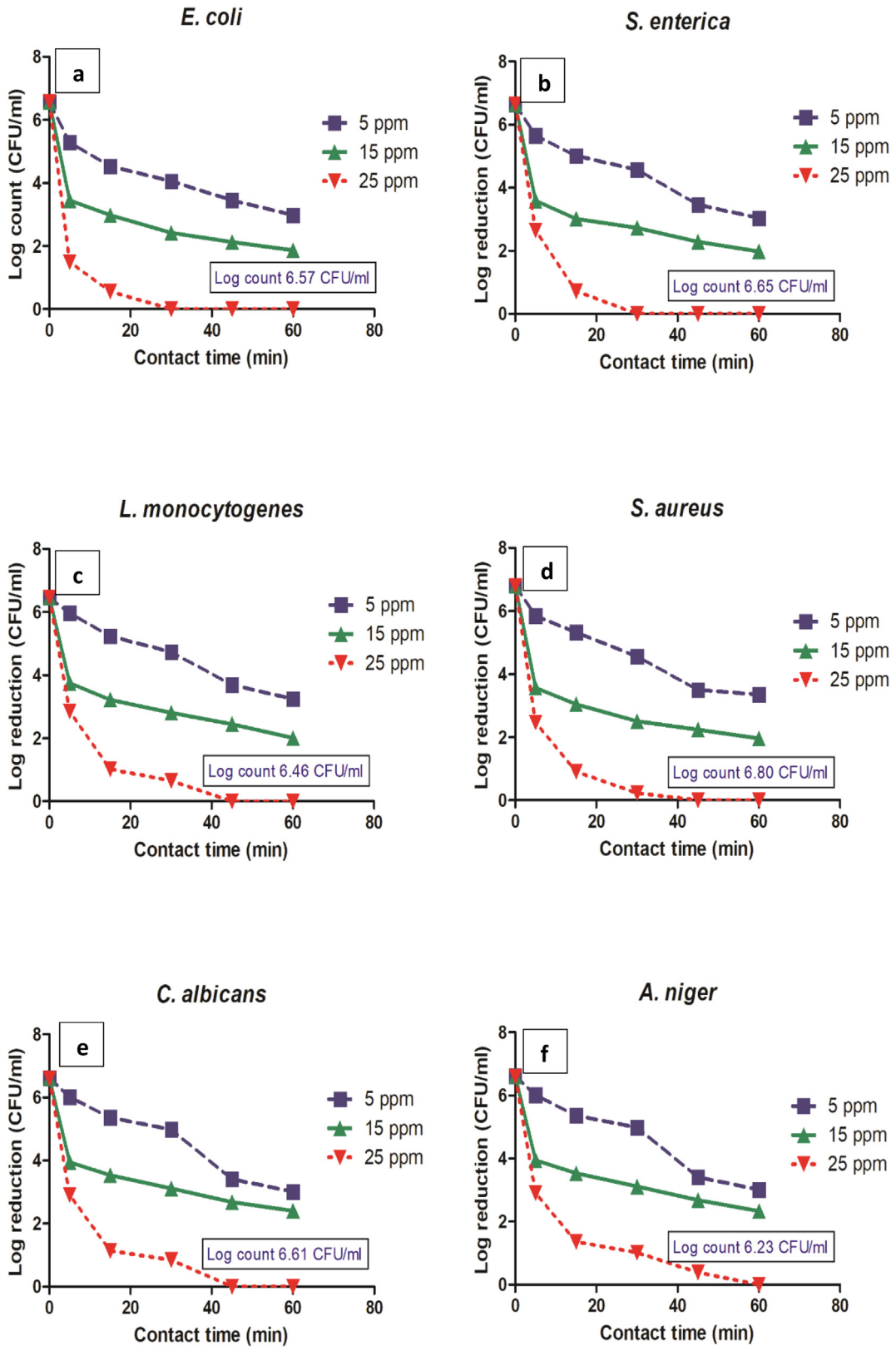

Fig. 8. Cell viability and log reduction of tested harmful microbial lineages (a) *E. coli*, (b) *S. enterica*, (c) *L. monocytogenes*, (d) *S. aureus*, (e) *C. albicans*, (f) *A. niger* inactivated by different doses of MNPs within various exposure times.

3.8. Application of MNPs in water and wastewater treatment

The fabricated MNPs are naturally coated to ameliorate their colloidal constancy and water dispensability, and to afford excellent chemical structure for the addition of bioactive molecules [57]. Three different water samples (raw surface water, raw domestic wastewater and synthetic contaminated tap water) were disinfected by 25 ppm of MNPs within various exposure times. The physico-chemical properties of tested

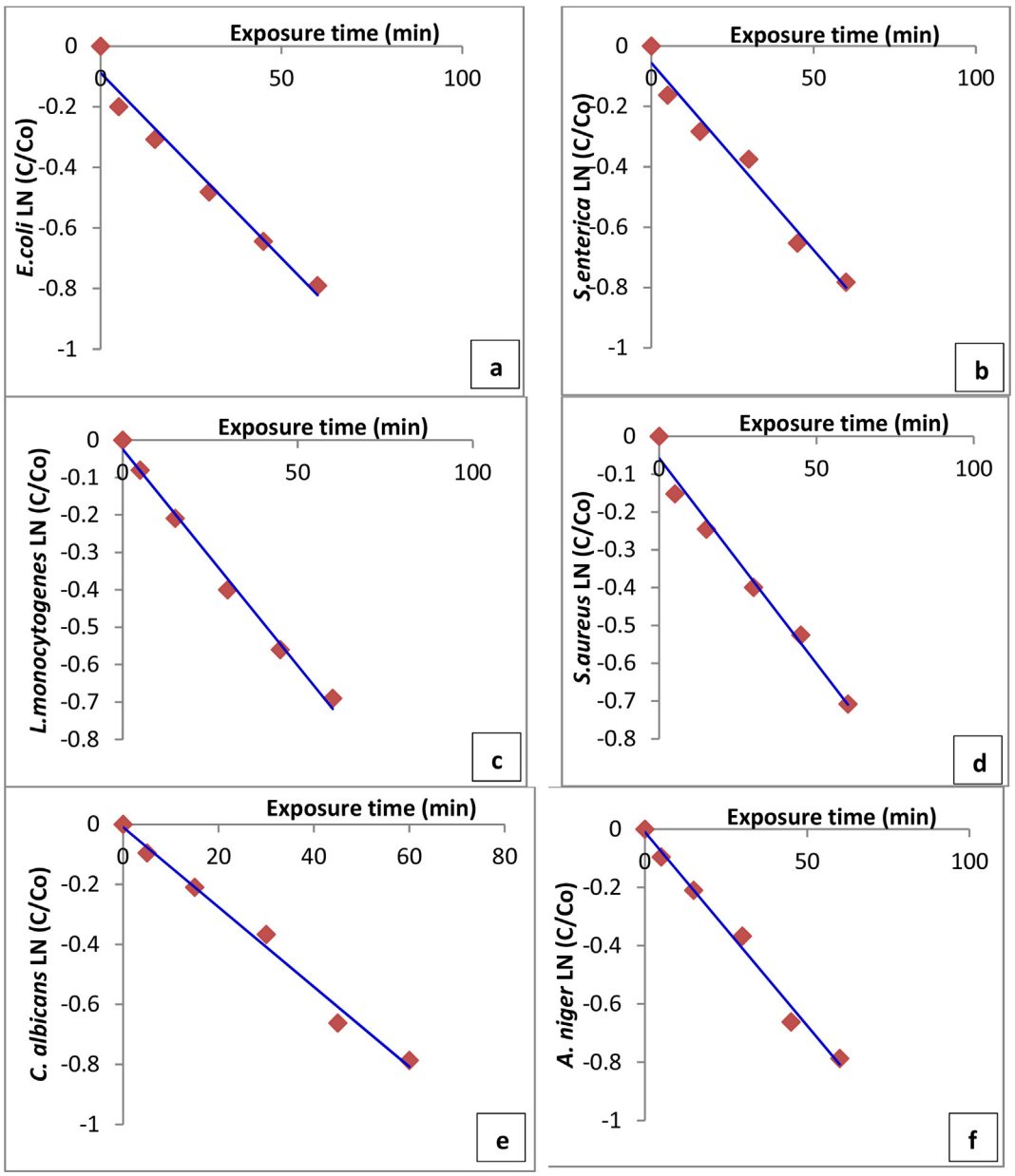

Fig. 9. Pseudo-first-order kinetic fitting of 5 ppm MNP-disinfectant at different exposure times for tested microbes (a) *E. coli*, (b) *S. enterica*, (c) *L. monocytogenes*, (d) *S. aureus*, (e) *C. albicans*, (f) *A. niger*.

water samples were estimated to characterize these samples before exposure to MNPs dosage (Table 3).

The population numbers of eight problematic microbes were estimated in all tested water samples. For low initial load of microbial populations (around log 3.3–3.7 CFU/ml) in raw Nile surface water, the complete log reduction was recorded for all estimated microbes after 10 min for Gram-negative bacteria, 15 min for Gram-positive bacteria and *C. albicans* and 30 min for *A. niger* (Table 4).

Table 2
Kinetic values (K_1(min^{-1})) of Pseudo-first-order calculation for inactivation of tested harmful microbial lineages by fabricated MNPs.

Tested microbial pathogens	MNPs dose			
	5 ppm		15 ppm	
	K_1	R^2	K_1	R^2
E. coli	0.0882	0.9688	0.3673	0.7725
S. enterica	0.0558	0.9737	0.3507	0.7698
L. monocytogenes	0.0247	0.9931	0.3001	0.8133
S. aureus	0.0379	0.9812	0.2981	0.9812
C. albicans	0.0099	0.9888	0.2848	0.786
A. niger	0.0098	0.9886	0.2803	0.8004

Table 3
Physico-chemical properties of the three tested water samples.

Items	Unit	Tested water samples		
		Raw Nile water	Raw wastewater	Synthetic DW
Physic-chemical properties				
pH		7.8	8.2	7.4
Turbidity	NTU	1.2	14	–
COD	mgO_2/L	17	145	–
BOD_5	mgO_2/L	7	84	–
TSS	mg/L	323	858	112
TDS	mg/L	476	1250	224
Iron	mg/L	0.8	4.5	–
Manganese	mg/L	0.1	3.4	–
Oil & grease	mg/L	0.82	7.6	–

TSS = Total suspended solids, TDS = Total dissolved solids.

Table 4
Cell viability and log counts of tested harmful microbial lineages disinfected with 25 ppm of MNPs within different exposure time in raw (Nile) surface water.

Detected microbes	Counts (CFU/ml)	Dosage of MNPs-disinfectant Exposure time (min)						
		0	5	10	15	30	45	60
E. coli	L.C	3.748	0.954	0	0	0	0	0
	L.R	0	2.794	3.748	3.748	3.748	3.748	3.748
S. enterica	L.C	3.531	1.023	0	0	0	0	0
	L.R	0	2.508	3.531	3.531	3.531	3.531	3.531
P. aeruginosa	L.C	3.612	0.956	0	0	0	0	0
	L.R	0	2.656	3.612	3.612	3.612	3.612	3.612
S. aureus	L.C	3.579	1.854	1.514	0	0	0	0
	L.R	0	1.725	2.065	3.579	3.579	3.579	3.579
L. monocytogenes	L.C	3.361	1.934	1.295	0	0	0	0
	L.R	0	1.427	2.066	3.361	3.361	3.361	3.361
E. faecalis	L.C	3.491	1.783	1.363	0	0	0	0
	L.R	0	1.708	2.128	3.491	3.491	3.491	3.491
C. albicans	L.C	3.491	1.783	1.363	0	0	0	0
	L.R	0	1.628	1.792	3.748	3.748	3.748	3.748
A. niger	L.C	3.534	2.307	1.783	0.563	0	0	0
	L.R	0	1.224	1.748	2.968	3.531	3.531	3.531

L.C = Log counts, L.R = Log reduction.

Table 5
Cell viability and log counts of tested harmful microbial lineages disinfected with 25 ppm of MNPs within different exposure time in raw domestic wastewater.

Detected microbes	Counts (CFU/ml)	Dosage of MNPs-disinfectant Exposure time (min)						
		0	5	10	15	30	45	60
E. coli	L.C	6.539	1.987	1.343	0.842	0	0	0
	L.R	0	4.552	5.196	5.697	6.539	6.539	6.539
S. enterica	L.C	6.322	2.342	1.893	1.213	0	0	0
	L.R	0	3.98	4.429	5.109	6.322	6.322	6.322
P. aeruginosa	L.C	5.716	2.547	2.083	1.086	0	0	0
	L.R	0	3.169	3.633	4.63	5.716	5.716	5.716
S. aureus	L.C	5.579	2.520	2.349	1.231	0.876	0	0
	L.R	0	3.059	3.23	4.348	4.703	5.579	5.579
L. monocytogenes	L.C	5.748	3.034	2.720	1.428	0.581	0	0
	L.R	0	2.714	3.028	4.32	5.167	5.748	5.748
E. faecalis	L.C	6.623	3.167	2.674	2.245	0.783	0	0
	L.R	0	3.456	3.949	4.378	5.84	6.623	6.623
C. albicans	L.C	6.534	3.624	3.083	2.504	0.915	0	0
	L.R	0	2.91	3.451	4.03	5.619	6.534	6.534
A. niger	L.C	6.322	3.946	3.210	2.738	1.201	0.729	0
	L.R	0	2.376	3.112	3.584	5.121	5.593	6.322

L.C = Log counts, L.R = Log reduction.

Table 6
Cell viability and log counts of tested harmful microbial lineages disinfected with 25 ppm of MNPs within different exposure time in synthetic contaminated drinking water.

Detected microbes	Counts (CFU/ml)	Dosage of MNPs-disinfectant Exposure time (min)						
		0	5	10	15	30	45	60
E. coli	L.C	6.53	2.014	1.801	0.740	0	0	0
	L.R	0	4.516	4.729	5.79	6.53	6.53	6.53
S. enterica	L.C	6.32	2.764	2.293	1.033	0	0	0
	L.R	0	3.556	4.027	5.287	6.32	6.32	6.32
P. aeruginosa	L.C	5.716	2.877	2.395	0.928	0	0	0
	L.R	0	2.839	3.321	4.788	5.716	5.716	5.716
S. aureus	L.C	5.579	2.952	2.791	2.131	1.514	0	0
	L.R	0	2.627	2.788	3.448	4.065	5.579	5.579
L. monocytogenes	L.C	5.748	3.570	2.907	2.028	1.295	0	0
	L.R	0	2.178	2.841	3.72	4.453	5.748	5.748
E. faecalis	L.C	6.623	3.146	2.818	1.803	1.363	0	0
	L.R	0	3.477	3.805	4.82	5.26	6.623	6.623
C. albicans	L.C	6.531	4.246	2.818	2.224	1.956	0	0
	L.R	0	2.285	3.713	4.307	4.575	6.531	6.531
A. niger	L.C	6.322	4.546	3.818	2.503	2.163	1.071	0
	L.R	0	1.776	2.504	3.819	4.159	5.251	6.322

L.C = Log counts, L.R = Log reduction.

As shown in Tables 5 and 6, under static condition (250 rpm shaking and 25 °C) and different exposure time, the viable cell counts were estimated for tested microbial lineages in raw domestic wastewater and synthetic contaminated DW samples before and after treatment with 25 ppm. After 30 min of exposure time, there was no any living bacterial cells (full eradication) of Gram-negative bacteria are present in treated sample. While Gram-negative bacteria need to a bit of long time up to 45 min to fully eradicate. In case of *A. niger*, the complete log reduction was observed after 60 min of exposure time.

The bactericidal efficacy could be displayed in brief in the following order: *E. coli* > coliforms > *Enterococcus* species > Gram-positive bacteria [48]. TiO_2 can deactivate both Gram-negative and Gram-positive bacteria; however, it has been stated that extreme Gram-positive bacteria have unveiled a powerful resistance to TiO_2, that could be credited to their spores formation ability [49]. While there is no strain that showed full removal of evolution, the elimination percentages were about 93%–99.5% for magnetic nanoparticles as opposed to *E. coli* and *Listeria* sp. after 2 hours of subjection, respectively. The results of the wastewater disinfection studies showed that MTUF has remarkable antimicrobial behavior in the water and wastewater remediation treatment approach [46].

4. Conclusion

The particle nanosize of $Zn_2Ti_{0.8}Fe_{0.2}O_4$ has been controlled successfully during calcination at 800 °C, which form dense and homogeneous nanoparticles. The phase of cubic structure $Zn_2Ti_{0.8}Fe_{0.2}O_4$ was identified using X-ray diffraction and the crystallite size is 55 nm. FE-SEM results reveal that dense Zn2Ti0.8Fe0.2 O'4 nanoparticles had been formed with high surface area and average particle size is ~60 nm. The dielectric constant decreases and the conductivity increases of $Zn_2Ti_{0.8}Fe_{0.2}O_4$ with increasing the frequency, also the loss tangent attains high values at low frequency. An obvious the absorption coefficient increases and shifted towards a higher THz frequency and the refractive index at the lower THz is higher than at the optical frequency for $Zn_2Ti_{0.8}Fe_{0.2}O_4$ nano-particles were seen when applying the external applied field. The dielectric and terahertz results should be a good reference for the future research of the optical field.

Antimicrobial susceptibility testing demonstrated that MNPs had an excellent potential to deactivate tested dangerous microbial strains. Results indicate that nano-particles $Zn_2Ti_{0.8}Fe_{0.2}O_4$ are non-toxic and safeguard for humans. MNPs are therefore regarded as an affordable and exceptional candidate for the disinfection during water and wastewater treatment of ubiquitous damaging microbial superbugs. MNPs could also be recovered from the water and recycled many times in the treatment of water and wastewater.

Declarations

Author contribution statement

Amany Mohamed El Nahrawy: Conceived and designed the experiments; Analyzed and interpreted the data; Contributed reagents, materials, analysis tools or data; Wrote the paper.

Ali Belal Abou Hammad & Ahmed Mohamed Bakr: Performed the experiments; Analyzed and interpreted the data; Contributed reagents, materials, analysis tools or data; Wrote the paper.

Bahaa Ahmed Hemdan: Analyzed and interpreted the data; Contributed reagents, materials, analysis tools or data; Wrote the paper.

Ahmed Ramzy Wassel: Contributed reagents, materials, analysis tools or data.

Funding statement

This work was supported by the Science and Technology Development Fund (STDF), Egypt (Project ID 25776).

Competing interest statement

The authors declare no conflict of interest.

Additional information

No additional information is available for this paper.

References

[1] Y.L.F. Musico, C.M. Santos, M.L.P. Dalida, D.F. Rodrigues, Surface modification of membrane filters using graphene and graphene oxide-based nanomaterials for bacterial inactivation and removal, ACS Sustain. Chem. Eng. (2014).
[2] G. Sharma, A. Kumar, M. Naushad, A. Kumar, A.H. Al-Muhtaseb, P. Dhiman, A.A. Ghfar, F.J. Stadler, M.R. Khan, Photoremediation of toxic dye from aqueous environment using monometallic and bimetallic quantum dots based nanocomposites, J. Clean. Prod. 172 (2018) 2919–2930.
[3] V.K. Sharma, T.J. McDonald, H. Kim, V.K. Garg, Magnetic graphene-carbon nanotube iron nanocomposites as adsorbents and antibacterial agents for water purification, Adv. Colloid Interface Sci. (2015).
[4] L. Peng, T. Xie, Y. Lu, H. Fan, D. Wang, Synthesis, photoelectric properties and photocatalytic activity of the Fe2O3/TiO2heterogeneous photocatalysts, Phys. Chem. Chem. Phys. (2010).
[5] A.B. Cundy, L. Hopkinson, R.L.D. Whitby, Use of iron-based technologies in contaminated land and groundwater remediation: a review, Sci. Total Environ. (2008).
[6] T. Esakkimuthu, D. Sivakumar, S. Akila, Application of nanoparticles in wastewater treatment, Pollut. Res. (2014).
[7] J.G. Lamori, J. Xue, A.T. Rachmadi, G.U. Lopez, M. Kitajima, C.P. Gerba, I.L. Pepper, J.P. Brooks, S. Sherchan, Removal of fecal indicator bacteria and antibiotic resistant genes in constructed wetlands, Environ. Sci. Pollut. Res. (2019).
[8] P. Xu, G.M. Zeng, D.L. Huang, C.L. Feng, S. Hu, M.H. Zhao, C. Lai, Z. Wei, C. Huang, G.X. Xie, Z.F. Liu, Use of iron oxide nanomaterials in wastewater treatment: a review, Sci. Total Environ. (2012).
[9] F. Hossain, O.J. Perales-Perez, S. Hwang, F. Román, Antimicrobial nanomaterials as water disinfectant: applications, limitations and future perspectives, Sci. Total Environ. (2014).
[10] G.S. Reddy, M.N. Nadagouda, J.A. Sekhar, Nanostructured surfaces that show antimicrobial, anticorrosive, and antibiofilm properties, Key Eng. Mater. (2012).
[11] M. Thakur, G. Sharma, T. Ahamad, A.A. Ghfar, D. Pathania, M. Naushad, Efficient photocatalytic degradation of toxic dyes from aqueous environment using gelatin-Zr(IV) phosphate nanocomposite and its antimicrobial activity, Colloids Surfaces B Biointerfaces (2017).
[12] S.C.N. Tang, I.M.C. Lo, Magnetic nanoparticles: essential factors for sustainable environmental applications, Water Res. (2013).
[13] S.A. Onaizi, S.S.J. Leong, Tethering antimicrobial peptides: current status and potential challenges, Biotechnol. Adv. (2011).
[14] A.M. El Nahrawy, A.B.A. Hammad, A.M. Bakr, A.R. Wassel, Adjustment of morphological and dielectric properties of ZnTiO3 nanocrystalline using Al2O3 nanoparticles, Appl. Phys. A 125 (2019) 54.
[15] Q. Xu, M. Järn, M. Lindén, J.H. Smått, Nanopatterned zinc titanate thin films prepared by the evaporation-induced self-assembly process, Thin Solid Films 531 (2013) 222–227.
[16] J. Qu, D. Huang, X. Wei, F. Liu, C. Yuan, B. Qin, Effect of NdAlO3 on microstructure, dielectric properties and temperature-stable mechanism of (Sr, Ca, Nd)TiO3 ceramics at microwave frequency, J. Mater. Sci. Mater. Electron. (2016).
[17] J. Ji, J. Yue, S. Zhou, Y. Tian, J. Zhang, F. Ling, H. Wang, C. Luo, J. Yao, Electrically tuned transmission and dielectric properties of illuminated and non-illuminated barium titanate thin film in terahertz regime, J. Alloy. Comp. (2018).
[18] J. Hudzicki, Kirby-Bauer Disk Diffusion Susceptibility Test Protocol, 2009.
[19] B.A. Hemdan, A.M. El Nahrawy, A.-F.M. Mansour, A.B.A. Hammad, Green sol–gel synthesis of novel nanoporous copper aluminosilicate for the eradication of pathogenic microbes in drinking water and wastewater treatment, Environ. Sci. Pollut. Res. (2019).
[20] W. El Hotaby, H.H.A. Sherif, B.A. Hemdan, W.A. Khalil, S.K.H. Khalil, Assessment of in situ-prepared polyvinylpyrrolidone-silver nanocomposite for antimicrobial applications, Acta Phys. Pol. 131 (2017) 1554–1560.
[21] American Public Health Association, American Water Works Association, Water Environment Federation, 9221 multiple-tube fermentation technique for members of the coliform group, in: Online (Ed.), Stand. Methods Exam. Water Wastewater, 2017. (Accessed 16 January 2017).
[22] T.S. Jamil, E.S. Mansor, M. Azab El-Liethy, Photocatalytic inactivation of E. coli using nano-size bismuth oxyiodide photocatalysts under visible light, J. Environ. Chem. Eng. (2015).
[23] T.S. Jamil, T.A. Gad-Allah, M.E.M. Ali, M.N.B. Momba, Utilization of nano size TiO2 for degradation of phenol enrich water by solar photocatalytic oxidation, Desalin. Water Treat. (2015).
[24] O.J. Hao, Lin Cheng-fang, Jeng Fu-Tien, Shih Chien-Jen, A review of Microtox test and its applications, Toxicol. Environ. Chem. (1995).
[25] J. Elith, J.R. Leathwick, Species distribution models: ecological explanation and prediction across space and time, Annu. Rev. Ecol. Evol. Syst. (2009).
[26] A.A. I, M.M.E. Ii, M.F.Z. Iii, A.B.A.H. I, Morphological Properties of Polycrystalline Perovskite Pbti3 Nanoparticles with High Purity Formed by Sol-Gel Technique vol. 4, 2017, pp. 1–4.

[27] C.-L. Wang, W.-S. Hwang, H.-L. Chu, C.-S. Hsi, H.-H. Ko, K.-M. Chang, X. Zhao, M.-C. Wang, W.-L. Li, Phase formation of zinc titanate precursor prepared by a hydrothermal route at pH 5, Ceram. Int. (2014).
[28] C.L. Wang, W.S. Hwang, H.H. Ko, C.S. Hsi, K.M. Chang, M.C. Wang, Phase transformation and microstructure of Zn2Ti3O8nanocrystallite powders prepared using the hydrothermal process, Metall. Mater. Trans. A Phys. Metall. Mater. Sci. (2014).
[29] K.H. Reddy, S. Martha, K.M. Parida, Fabrication of novel p-BiOI/n-ZnTiO3heterojunction for degradation of rhodamine 6G under visible light irradiation, Inorg. Chem. (2013).
[30] K. Akhtar, M. Gul, I.U. Haq, S.S.A. Shah, Z.U. Khan, Effect of calcination temperature on the morphological and dielectric properties of phase-pure MnCrFeO4nanoparticles, Inorg. Nano-Metal Chem. (2017).
[31] A.M. ElNahrawy, A.A. Haroun, I. Hamadneh, A.H. Al-Dujaili, S. kamel, Conducting cellulose/TiO2composites by in situ polymerization of pyrrole, Carbohydr. Polym. (2017).
[32] A.M.E. Nahrawy, A.A. Haroun, A.B.A. Hammad, M.A. Diab, S. Kamel, Uniformly Embedded Cellulose/Polypyrrole-TiO2Composite in Sol-Gel Sodium Silicate Nanoparticles: Structural and Dielectric Properties, Silicon, 2018, pp. 1–8.
[33] M. Chaari, R. Ben Belgacem, A. Matoussi, Impedance analysis , dielectric relaxation and modulus behaviour of ZnO-Sn 2 O 3 ceramics, J. Alloy. Comp. 726 (2017) 49–56.
[34] R.S. Yadav, I. Kuřitka, J. Vilcakova, P. Urbánek, M. Machovsky, M. Masař, M. Holek, Structural, magnetic, optical, dielectric, electrical and modulus spectroscopic characteristics of ZnFe2O4spinel ferrite nanoparticles synthesized via honey-mediated sol-gel combustion method, J. Phys. Chem. Solids (2017).
[35] Y.J. Wong, J. Hassan, M. Hashim, Dielectric properties, impedance analysis and modulus behavior of CaTiO3 ceramic prepared by solid state reaction, J. Alloy. Comp. (2013).
[36] S. Bhardwaj, J. Paul, K.K. Raina, N.S. Thakur, R. Kumar, Dielectric modulus and magnetocapacitance behavior of Bi3.7Sm0.3Ti2.7Fe0.3O12multiferroic, Phys. B Condens. Matter (2014).
[37] S.W. Yun, J.H. Koh, The ac conductivity and complex impedance of CuO-doped (Ba0.5Sr0.5)TiO3ceramic, J. Phys. Chem. Solids (2012).
[38] M. Abdessalem, A. Aydi, N. Abdelmoula, Raman scattering , structural , electrical studies and conduction, J. Alloy. Comp. 774 (2019) 685–693.
[39] R. Qindeel, N.H. Alonizan, Structural, dielectric and magnetic properties of cobalt based spinel ferrites, Curr. Appl. Phys. 18 (2018) 519–525.
[40] A. Ravagli, M. Naftaly, C. Craig, E. Weatherby, D.W. Hewak, Dielectric and structural characterisation of chalcogenide glasses via terahertz time-domain spectroscopy, Opt. Mater. (Amst) (2017).
[41] S. Kojima, H. Kitahara, S. Nishizawa, M. Wada Takeda, Dielectric properties of ferroelectric lithium tantalate crystals studied by terahertz time-domain spectroscopy, Japanese, J. Appl. Physics, Part 1 Regul. Pap. Short Notes Rev. Pap. (2003).
[42] K.-S. Huang, P.-C. Wu, C.-S. Yeh, D.-B. Shieh, F.-Y. Cheng, Antimicrobial applications of water-dispersible magnetic nanoparticles in biomedicine, Curr. Med. Chem. (2014).
[43] L. Mohammed, H.G. Gomaa, D. Ragab, J. Zhu, Magnetic nanoparticles for environmental and biomedical applications: a review, Particuology (2017).
[44] C. Wei, W.Y. Lin, Z. Zainal, N.E. Williams, K. Zhu, A.P. Kruzlc, R.L. Smith, K. Rajeshwar, Bactericidal activity of TiO2 photocatalyst in aqueous media: toward a solar-assisted water disinfection system, Environ. Sci. Technol. (1994).
[45] N. Jones, B. Ray, K.T. Ranjit, A.C. Manna, Antibacterial activity of ZnO nanoparticle suspensions on a broad spectrum of microorganisms, FEMS Microbiol. Lett. (2008).
[46] K.Z. Elwakeel, M.A. El-Liethy, M.S. Ahmed, S.M. Ezzat, M.M. Kamel, Facile synthesis of magnetic disinfectant immobilized with silver ions for water pathogenic microorganism's deactivation, Environ. Sci. Pollut. Res. (2018).
[47] M.R. Bindhu, M. Umadevi, Silver and gold nanoparticles for sensor and antibacterial applications, Spectrochim. Acta Part A Mol. Biomol. Spectrosc. (2014).
[48] A. Markowska-Szczupak, K. Ulfig, A.W. Morawski, The application of titanium dioxide for deactivation of bioparticulates: an overview, Catal. Today (2011).
[49] Y. Liu, J. Li, X. Qiu, C. Burda, Bactericidal activity of nitrogen-doped metal oxide nanocatalysts and the influence of bacterial extracellular polymeric substances (EPS), J. Photochem. Photobiol. A Chem. (2007).
[50] K.P. Kühn, I.F. Chaberny, K. Massholder, M. Stickler, V.W. Benz, H.G. Sonntag, L. Erdinger, Disinfection of surfaces by photocatalytic oxidation with titanium dioxide and UVA light, Chemosphere (2003).
[51] B.R. Flokstra, B. Van Aken, J.L. Schnoor, Microtox® toxicity test: detoxification of TNT and RDX contaminated solutions by poplar tissue cultures, Chemosphere 71 (2008) 1970–1976.
[52] G.W. Ali, W. El-Hotaby, B. Hemdan, W.I. Abdel-Fattah, Thermosensitive chitosan/phosphate hydrogel-composites fortified with Ag versus Ag@Pd for biomedical applications, Life Sci. (2018).
[53] A. Elsaesser, C.V. Howard, Toxicology of nanoparticles, Adv. Drug Deliv. Rev. (2012).
[54] World Health Organization, Guidelines for Drinking-Water Quality, fourth ed., 2011.
[55] H. Arami, A. Khandhar, D. Liggitt, K.M. Krishnan, In Vivo delivery, pharmacokinetics, biodistribution and toxicity of iron oxide nanoparticles, Chem. Soc. Rev. (2015).
[56] S.T. Gaballah, H.A. El-Nazer, R.A. Abdel-Monem, M.A. El-Liethy, B.A. Hemdan, S.T. Rabie, Synthesis of novel chitosan-PVC conjugates encompassing Ag nanoparticles as antibacterial polymers for biomedical applications, Int. J. Biol. Macromol. 121 (2019) 707–717.
[57] A.J. Cole, V.C. Yang, A.E. David, Cancer theranostics: the rise of targeted magnetic nanoparticles, Trends Biotechnol. (2011).